Acta Crystallographica Section F
Structural Biology and Crystallization Communications
ISSN 1744-3091

The precursor form of *Hansenula polymorpha* copper amine oxidase 1 in complex with Cu^{I} and Co^{II}

Valerie J. Klema,[a] Bryan J. Johnson,[a]‡ Judith P. Klinman[b] and Carrie M. Wilmot[a]*

[a]Department of Biochemistry, Molecular Biology and Biophysics, University of Minnesota, 321 Church Street SE, Minneapolis, MN 55455, USA, and [b]Department of Chemistry and Department of Molecular and Cell Biology, and the California Institute of Quantitative Biosciences (QB3), University of California, 608C Stanley Hall, Berkeley, CA 94720, USA

‡ Current address: R&D Systems Inc., 614 McKinley Place NE, Minneapolis, MN 55413, USA.

Correspondence e-mail: wilmo004@umn.edu

Received 5 March 2012
Accepted 23 March 2012

PDB References: apoHPAO-1, 3sx1; Co^{II}–apoHPAO-1, 3sxx; Cu^{I}–apoHPAO-1, 3t0u.

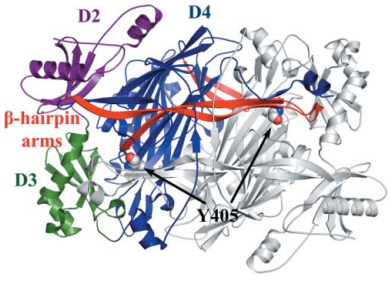

Copper amine oxidases (CAOs) catalyze the oxidative deamination of primary amines to their corresponding aldehydes, with the concomitant reduction of O_2 to H_2O_2. Catalysis requires two cofactors: a mononuclear copper center and the cofactor 2,4,5-trihydroxyphenylalanine quinone (TPQ). TPQ is synthesized through the post-translational modification of an endogenous tyrosine residue and requires only oxygen and copper to proceed. TPQ biogenesis in CAO can be supported by alternate metals, albeit at decreased rates. A variety of factors are thought to contribute to the degree to which a metal can support TPQ biogenesis, including Lewis acidity, redox potential and electrostatic stabilization capability. The crystal structure has been solved of one of two characterized CAOs from the yeast *Hansenula polymorpha* (HPAO-1) in its metal-free (apo) form, which contains an unmodified precursor tyrosine residue instead of fully processed TPQ (HPAO-1 was denoted HPAO in the literature prior to 2010). Structures of apoHPAO-1 in complex with Cu^{I} and Co^{II} have also been solved, providing structural insight into metal binding prior to biogenesis.

1. Introduction

Copper amine oxidases (CAOs) are ubiquitous homodimeric enzymes that are responsible for the two-electron oxidative deamination of primary amines to their corresponding aldehydes. Found in aerobic organisms ranging from bacteria to higher eukaryotes, the physiological roles of CAOs and their sources are diverse. In bacteria and yeast CAOs play a mainly metabolic role, enabling the use of primary amines as a sole source of carbon and/or nitrogen for growth (Wilce *et al.*, 1997; Green *et al.*, 1983). The functions of these enzymes in higher eukaryotes are not as well understood, with CAO being thought to contribute to a number of complex processes, including wound healing and cell-wall maturation in plants and inflammatory leukocyte extravasation, glucose regulation and cell signaling in mammals (Salmi *et al.*, 2001; Angelini *et al.*, 2010; Shen *et al.*, 2012). Aberrant human CAO activity has been linked to a number of disease states marked by protein cross-linking, including Alzheimer's disease, diabetic complications and congestive heart disease (Jiang *et al.*, 2008; Obata, 2006; Dunkel *et al.*, 2008).

Despite their wide variety of sources and biological functions, all CAOs catalyze the same chemistry: the oxidative deamination of primary amine substrates coupled to the reduction of O_2 to H_2O_2 in the following overall reaction (Salmi *et al.*, 2001; Cai & Klinman, 1994*a*; Janes *et al.*, 1990):

$$R\mathrm{CH_2NH_3^+} + \mathrm{O_2} + \mathrm{H_2O} \rightarrow R\mathrm{CHO} + \mathrm{NH_4^+} + \mathrm{H_2O_2}.$$

CAOs are members of a growing number of bifunctional enzymes which synthesize their own organic cofactors *de novo* (Davidson, 2007). This increases the diversity of chemical properties available in an enzyme active site beyond that of the 20 canonical amino-acid side chains. In the case of CAO, the redox-active cofactor 2,4,5-trihydroxyphenylalanine quinone (TPQ) is produced autocatalytically by the oxidation of an endogenous tyrosine residue (Fig. 1; Janes *et al.*, 1990; Matsuzaki *et al.*, 1994; Cai & Klinman, 1994*b*). This process occurs without auxiliary proteins and requires only the presence of oxygen and copper.

Understanding the role of copper is necessary for a complete picture of TPQ biogenesis in CAOs. Previous spectroscopic, kinetic and structural studies suggest a critical role for copper *via* its direct ligation by the precursor tyrosine residue. In HPAO-1, this is thought to activate the phenolic ring for monooxygenation by pre-bound molecular oxygen in a nearby site (Dove *et al.*, 2000; Schwartz *et al.*, 2000; Chen *et al.*, 2000). It had previously been believed that only copper, the physiologically relevant metal in CAO, could support the biogenesis of TPQ. Work performed with metal-free precursor CAO from the yeast *Hansenula polymorpha* (HPAO-1) and the bacterium *Arthrobacter globiformis* (AGAO) has challenged this, revealing that alternate metals can support TPQ formation *in vitro*, albeit at decreased rates (Table 1; Samuels & Klinman, 2005, 2006; Okajima *et al.*, 2005; Dove *et al.*, 2000). In HPAO-1, the biogenesis of TPQ can proceed with Cu^{II}, Cu^{I} or Ni^{II} bound at the metal-binding site, but is not supported by Co^{II} (Samuels & Klinman, 2005, 2006; Dove *et al.*, 2000). In contrast, TPQ biogenesis in AGAO is supported by bound active-site Co^{II} as well as Cu^{II} and Ni^{II} (Okajima *et al.*, 2005). Zn^{II} is unable to promote TPQ biogenesis in CAOs and furthermore resists displacement by copper when bound to the CAO active site (Cai *et al.*, 1997; McGrath *et al.*, 2010).

The initial assumption that it was necessary to fully reduce Cu^{II} to form a Cu^{I}-tyrosinate species for tyrosine-ring activation has been challenged by studies using metal-free precursor (apo) AGAO (apoAGAO) and HPAO-1 (apoHPAO-1) (Samuels & Klinman, 2006). Although TPQ biogenesis is supported by Ni^{II} and Co^{II} in AGAO, the very low reduction potentials for both the Ni^{II}/Ni^{I} [−1.16 V *versus* the standard hydrogen electrode (SHE) in complexes with N/O ligands] and Co^{II}/Co^{I} (for example, −0.4 to −0.5 V *versus* SHE in methionine synthase) couples would disfavor a mechanism which requires reduction of the metal by the TPQ precursor tyrosine (Drummond & Matthews, 1994; Gomes *et al.*, 2000). Kinetic measurements of TPQ biogenesis in apoHPAO-1 indicate that TPQ is produced in Cu^{I}-supplemented apoHPAO-1 protein at a rate 17-fold slower than in Cu^{II}-supplemented apoHPAO-1, which is ascribed to an initial requisite oxidation of Cu^{I} to Cu^{II} (Samuels & Klinman, 2006). Additionally, in a study of Ni^{II}-initiated cofactor production in apoHPAO-1, EPR spectroscopy revealed that the bulk of the bound nickel is EPR silent, which is consistent with a +2 oxidation state being maintained throughout biogenesis (Samuels & Klinman, 2005). These studies disfavor a mechanism in which Cu^{II} must first be fully reduced to Cu^{I} for the initiation of cofactor biogenesis (Samuels & Klinman, 2005). The fact that HPAO-1 is localized to the *H. polymorpha* peroxisome, together with the lack of free copper or copper transporters associated with this organelle, suggests that copper is initially inserted into apoHPAO-1 in the reducing cytosol as Cu^{I} before subsequent oxidation to Cu^{II} and TPQ biogenesis (Puig & Thiele, 2002; Faber *et al.*, 1994; Hassett & Kosman, 1995).

In light of these data, Lewis acidity has been proposed to contribute to the ability of a metal to support cofactor biogenesis, as Cu^{II} is a better Lewis acid than Co^{II} and Ni^{II} (Samuels & Klinman, 2005; Okajima *et al.*, 2005). However, this does not explain the complete inactivity with the effective Lewis acid Zn^{II} bound at the active site (Chen *et al.*, 2000). Thus, the inherent reduction potential of a metal appears to play at least some part in metal specificity during biogenesis. Differences in the versatility of a metal's coordination sphere may act as additional factors which influence the ability of a metal to support TPQ formation (Chen *et al.*, 2000; Okajima *et al.*, 2005; Kishishita *et al.*, 2003). The current data regarding the role of metal in TPQ biogenesis suggest that a combination of several factors, including redox properties, Lewis acidity and electrostatic stabilization capabilities, contribute to the degree to which a metal can initiate and support TPQ biogenesis in CAO.

To visualize the initial step of biogenesis, the X-ray crystal structure of precursor HPAO-1 in the absence of metal (apoHPAO-1) has been solved to a resolution of 1.7 Å. In addition, X-ray crystal structures of apoHPAO-1 in complex with Cu^{I} and Co^{II} have been solved to resolutions of 1.9 and 1.27 Å, respectively, providing insight into the structural role of metals during biogenesis.

Table 1
k_{TPQ} for biogenesis in HPAO-1 and AGAO supported by various metals.

	HPAO-1 (h^{-1})	AGAO (h^{-1})
Cu^{II}	4.8 ± 0.2†	90 ± 12‡§
Cu^{I}	0.28 ± 0.06¶	Unmeasured
Ni^{II}	0.028 ± 0.006††	(7.5 ± 0.12) × 10^{-2}‡§
Co^{II}	Not supported	(7.92 ± 0.24) × 10^{-2}‡§
Zn^{II}	Not supported	Not supported

† Dove *et al.* (2000). ‡ Okajima *et al.* (2005). § Data originally reported in min^{-1}. ¶ Samuels & Klinman (2006). †† Samuels & Klinman (2005).

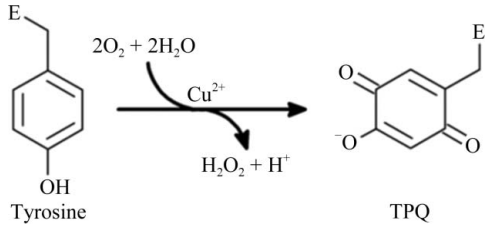

Figure 1
An endogenous tyrosine residue is converted to TPQ in an autocatalytic oxygen- and copper-dependent process. E represents the enzyme polypeptide.

2. Methods

2.1. Protein expression, purification and characterization

Metal-free apoHPAO-1 protein was expressed and purified in *Escherichia coli* as described previously (Dove *et al.*, 2000; Samuels & Klinman, 2005; McGrath *et al.*, 2010). Zinc is known to bind tightly to the HPAO-1 active site and to inhibit copper-mediated TPQ biogenesis (McGrath *et al.*, 2010). Therefore, to prepare functional precursor HPAO-1 which forms TPQ upon aerobic incubation with copper, the growth medium and the buffers used for apoHPAO-1 expression and purification were kept free of all divalent transition metals. All buffers and solutions were prepared using water with a resistance greater than 18 MΩ (Millipore Super-Q water-purification system). Plastic flasks and beakers used during *E. coli* growth and protein purification were soaked in an ethylenediaminetetraacetic acid (EDTA) bath (0.5 *M*) before thorough rinsing with metal-free water. The precursor protein (at 40 µ*M*) was assayed for TPQ-formation activity in 50 m*M* HEPES pH 7.0 by the addition of a $CuSO_4$ solution to a final concentration of 0.04 m*M*. Absorbance changes were monitored over the course of 1 h to visualize the appearance of a 480 nm absorbance feature indicating the formation of TPQ using a Cary 50-Bio spectrometer (Varian). ApoHPAO-1 protein at a concentration of 1.2 mg ml^{-1} in 50 m*M* HEPES was subjected to inductively coupled plasma-mass spectrometry (ICP-MS) at the University of Minnesota Aqueous Geochemistry Laboratory.

2.2. ApoHPAO-1 crystallization and preparation of apoHPAO-1–metal complexes

ApoHPAO-1 protein was buffer-exchanged into 50 m*M* HEPES pH 7.0 and concentrated to 13 mg ml^{-1} for crystallization. Crystals of

Table 2
X-ray data-collection, processing and refinement statistics for apoHPAO-1, Cu^{I}–apoHPAO-1 and Co^{II}–apoHPAO-1.

Values in parentheses are for the highest resolution shell.

	ApoHPAO-1	Cu^{I}–apoHPAO-1	Co^{II}–apoHPAO-1
PDB code	3sx1	3t0u	3sxx
Detector type	ADSC Quantum 315r	ADSC Quantum 315r	ADSC Quantum 315r
Beamline and source	19-ID, SBC-CAT, APS	19-ID, SBC-CAT, APS	19-ID, SBC-CAT, APS
Temperature (K)	100	100	100
Space group	$C222_1$	$C222_1$	$P2_1$
Unit-cell parameters (Å, °)	a = 139.6, b = 153.6, c = 223.6, β = 90	a = 139.4, b = 153.7, c = 223.5, β = 90	a = 103.9, b = 223.4, c = 104.0, β = 95.6
No. of molecules in unit cell (Z)	1.5	1.5	3
Wavelength (Å)	0.979	0.979	0.979
Resolution (Å)	50.00–1.73 (1.76–1.73)	50.00–1.90 (1.97–1.90)	50.00–1.27 (1.32–1.27)
No. of unique reflections	240796	187095	1169541
Completeness (%)	97.3 (88.1)	100.0 (99.8)	94.9 (85.3)
R_{merge}†	0.074 (0.447)	0.110 (0.448)	0.073 (0.357)
$\langle I/\sigma(I)\rangle$	32.3 (3.9)	17.9 (4.1)	23.5 (3.4)
Multiplicity	10.0 (8.7)	7.1 (6.8)	3.7 (3.4)
Refinement resolution range (Å)	31.61–1.73 (1.77–1.73)	49.14–1.90 (1.95–1.90)	31.70–1.27 (1.30–1.27)
No. of reflections in the working set	228647 (15773)	177631 (12933)	1110572 (72499)
No. of reflections in the test set	12085 (869)	9388 (664)	58671 (3854)
R_{work}‡ (%)	13.4 (20.2)	12.5 (16.8)	10.8 (17.4)
R_{free}§ (%)	16.3 (25.1)	17.5 (23.1)	13.8 (21.3)
No. of non-H atoms	18574	18804	39005
No. of amino-acid residues	1970	1990	3974
No. of protein atoms	15895	15949	32469
No. of solvent molecules	2584	2734	6250
No. of metal ions	0	3	6
No. of other atoms	95	119	280
Residues modeled	Ala16–Val672	Ala16–His673, Ala682–Gly691	Ala15–Val672, Leu683–Gly691
R.m.s.d. from ideal geometry			
Bond lengths (Å)	0.016	0.022	0.022
Bond angles (°)	1.53	1.96	1.96
Ramachadran plot			
Favored regions (%)	97.5	97.0	97.4
Allowed regions (%)	2.4	2.8	2.5
Outliers (%)	0.1	0.2	0.1
B factors (Å^2)			
Average	16.7	15.1	13.1
Main chain	13.2	11.4	8.7
Side chain	16.3	14.1	11.6
Ligands	40.8	36.6	26.9
Solvent atoms	28.1	30.5	27.3
Cruickshank's DPI (Å)	0.09	0.10	0.03

† $R_{merge} = \sum_{hkl}\sum_i |I_i(hkl) - \langle I(hkl)\rangle| / \sum_{hkl}\sum_i I_i(hkl)$, where $I_i(hkl)$ is the observed intensity and $\langle I(hkl)\rangle$ is the average intensity for multiple measurements. ‡ $R_{work} = \sum_{hkl} ||F_{obs}| - |F_{calc}|| / \sum_{hkl} |F_{obs}|$, where $|F_{obs}|$ is the observed structure-factor amplitude and $|F_{calc}|$ is the calculated structure-factor amplitude for 95% of the data used in refinement. § R_{free} is based on 5% of the data excluded from refinement.

apoHPAO-1 were grown by hanging-drop vapor diffusion using a 1:1 volume ratio (6 µl in total) of purified protein solution and crystallization solution (8–9.5% polyethylene glycol 8000, 0.28–0.30 *M* potassium phosphate, pH 6.0) which had been mixed and incubated with a small amount of Chelex (Bio-Rad) for at least 1 h to remove any divalent metals present in the crystallization solution. After equilibrating for ∼24 h, drops were seeded using a streak-seeding technique with a native mature HPAO-1 crystal as the seed donor. Colorless crystals grew to full size within 7–9 d. To eliminate the possibility of contamination from the native HPAO-1 protein seeds, a subsequent round of streak-seeding was performed using apoHPAO-1 crystals as seed donors. Cryoprotection for all crystals was performed by soaking in 25% high-purity glycerol mixed with well solution for ∼10 s before flash-cooling in liquid nitrogen.

The crystal of apoHPAO-1 in complex with Co^{II} was prepared by soaking an apoHPAO-1 crystal in crystallization solution containing 10 m*M* $CoCl_2$ for 1 h before cryoprotection and flash-cooling in liquid nitrogen. This soak was performed in ambient air as Co^{II} does not support TPQ formation and it was not necessary to work anaerobically to prevent the initiation of biogenesis.

To prepare crystals of an anaerobic complex of apoHPAO-1 with Cu^{I}, a solution of tetrakis(acetonitrile)copper(I) hexafluorophosphate was made anaerobic by passing high-purity nitrogen gas over the solution headspace while stirring for >10 min in a septa-covered vessel. This was immediately brought into an anaerobic glove box (Belle Technology). Trays containing apoHPAO-1 crystals were brought into the anaerobic glove box and allowed to equilibrate for at least one week. ApoHPAO-1 crystals were soaked in crystallization solution containing 5 m*M* tetrakis(acetonitrile)copper(I) hexafluorophosphate for 1 h before cryoprotection and flash-cooling in liquid nitrogen.

2.3. Data collection, structure solution and refinement

X-ray diffraction data were collected from single apoHPAO-1, Cu^{I}-apoHPAO-1 and Co^{II}-apoHPAO-1 crystals at 100 K at the Advanced Photon Source (APS), Argonne National Laboratory (beamline 19-ID, SBC-CAT) and were processed using *HKL*-2000 and *SCALEPACK* (Otwinowski & Minor, 1997). Two different apoHPAO-1 crystal polymorphs belonging to space groups $P2_1$ and $C222_1$ were found to grow from identical conditions (Li *et al.*, 1997). Difference Fourier techniques were used to produce initial electron-density maps for the Co^{II}–apoHPAO-1 structure in space group $P2_1$ using a previously deposited isomorphous HPAO-1 structure (PDB

entry 2oov with solvent molecules, metal and the side chain of TPQ removed; Johnson *et al.*, 2007) and programs within the *CCP*4 suite (Winn *et al.*, 2011). Structures in space group $C222_1$ (apoHPAO-1 and Cu^{I}–apoHPAO-1) were solved by molecular replacement using the program *Phaser* in the *CCP*4 suite with an HPAO-1 monomer from the structure of native HPAO-1 as a search model (PDB code 2oov with solvent molecules, metal and the side chain of TPQ removed). Manual model building was performed using *Coot* (Emsley & Cowtan, 2004) and refinement was carried out using the program *REFMAC* in the *CCP*4 suite (Murshudov *et al.*, 2011). Test refinements and *B*-factor matching were used to determine partial occupancies of alternate side-chain conformations and bound metal ions. This approach involves the systematic variation of the occupancy of the components by increments of 0.10 (keeping a combined occupancy of 1.0) and subsequent refinement. The resulting *B* factors for each set of contributing components were compared with those of surrounding well ordered side chains. The occupancies that best matched the *B* factors were assigned to the alternate conformers or metal ions. Refinement continued until peaks in the $F_o - F_c$ electron-density map were at the level of noise. The three apoHPAO-1 structures were validated with the programs *PROCHECK*, *NUCheck*, *SFCheck* and *MolProbity* (Laskowski *et al.*, 1993; Feng *et al.*, 1998; Vaguine *et al.*, 1999; Chen *et al.*, 2010). The final model coordinates and structure factors have been deposited in the PDB (http://www.rcsb.org) as entries 3sx1 (apoHPAO-1), 3t0u (Cu^{I}–apoHPAO-1) and 3sxx (Co^{II}–apoHPAO-1). Hydrogen bonds were defined by the program *CCP*4*MG* (McNicholas *et al.*, 2011) and structural figures were produced using the visualization program *PyMOL* (http://www.pymol.org).

3. Results

3.1. ApoHPAO-1 protein analysis

Purified apoHPAO-1 protein was assayed for TPQ biosynthetic activity by the aerobic addition of $CuSO_4$. UV–visible spectroscopic analysis showed an absorbance feature at 380 nm which formed initially and then disappeared with the subsequent formation of a broad absorbance feature at 480 nm corresponding to TPQ formation (Fig. 2). Metal quantification by ICP-MS indicated that apoHPAO-1 protein contained 0.001 Cu^{2+}, 0.005 Zn^{2+}, 0.0001 Co^{2+} and 0.0003 Ni^{2+} ions per monomer of apoHPAO-1.

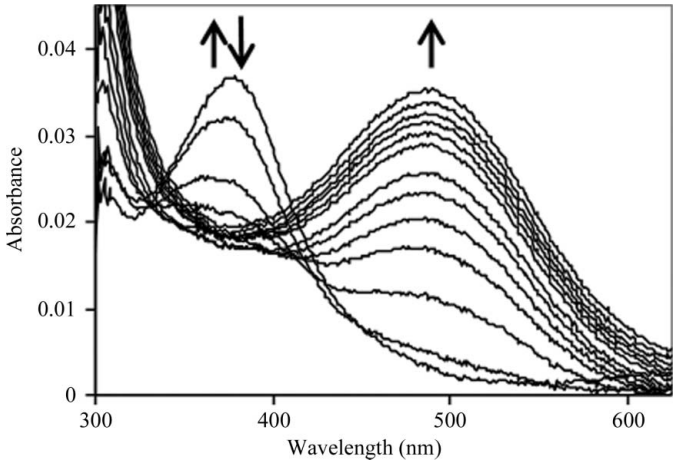

Figure 2
UV–visible spectra showing the time course of the aerobic reconstitution of apoHPAO-1 with Cu^{II} at pH 7.0. The directions of change for UV–visible absorbance features over time are indicated by arrows.

3.2. X-ray crystal structure analysis: overall fold

Table 2 contains X-ray crystallographic data-collection, processing and refinement statistics for apoHPAO-1 and apoHPAO-1 in complex with Cu^{I} and Co^{II}. The structure of Co^{II}–apoHPAO-1 contains six polypeptide chains, or three physiological HPAO-1 dimers, in the crystallographic asymmetric unit in space group $P2_1$, while those in space group $C222_1$ (apoHPAO-1 and Cu^{I}-apoHPAO-1) contain three chains or 1.5 physiological dimers in the asymmetric unit. The overall fold of all three structures is nearly identical to that of native HPAO-1 (PDB entry 2oov), with superimposition of corresponding main-chain atoms yielding root-mean-square deviations (r.m.s.d.s) of 0.29, 0.27 and 0.14 Å for apoHPAO-1, Cu^{I}-apoHPAO-1 and Co^{II}-apoHPAO-1, respectively. The structures of apoHPAO-1 and metal-bound apoHPAO-1 adopt the canonical CAO overall fold consisting of three domains (D2–D4) arranged along the primary sequence (Fig. 3). All significant structural differences between the metal complexes or apoHPAO-1 and the native HPAO-1 structure are localized to either the enzyme active site or the C-terminus.

3.3. X-ray crystal structure analysis: apoHPAO-1 active site

X-ray diffraction data were collected from crystals of apoHPAO-1 to a resolution of 1.7 Å (Table 2). Distances are reported as the range observed across the three polypeptides in the asymmetric unit following refinement. The HPAO-1 active site lies deeply buried within the protein interior. The absence of copper leaves room for an ordered water molecule at the metal-binding site (W in Fig. 4*a*). This water molecule is bound by His456 and His458 at distances of 2.8–2.9 Å as well as by the precursor tyrosine residue at a distance of 2.6–2.8 Å in a distorted tetrahedral geometry (Fig. 4*a*). The side chains of histidine residues 456 and 458 adopt the orientations observed in the structure of native HPAO-1. The third histidine residue (His624) is observed in two conformations. One is equivalent to that of native HPAO-1, but is only 2.1–2.3 Å from the water, suggesting that water can only occupy the site when His624 adopts the second conformation. The second conformer is oriented away from the empty metal site by a rotation of ∼90° around its $C^{\beta}-C^{\gamma}$ bond and is hydrogen-bonded to the carboxylate of Asp630. This alternate His624 conformer is present at varying occupancies within the three protein monomers located within the asymmetric unit

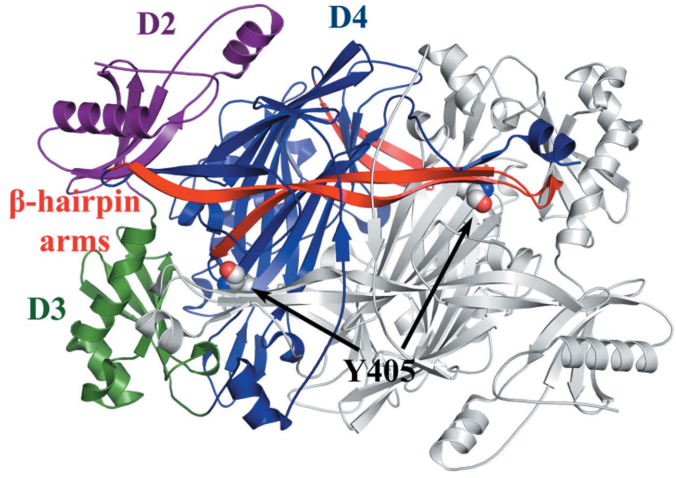

Figure 3
Arrangement of the domains and β-hairpin arms in apoHPAO-1. The structure of apoHPAO-1 is shown in cartoon representation, with one monomer colored by domain (D2, purple; D3, green; D4, blue; β-hairpin arms, red) and the other colored gray. The precursor tyrosine residues (Tyr405) from both monomers are shown as spheres and are colored by atom type (carbon, white).

(chain *A*, occupancy = 1.0; chain *B*, occupancy = 0.7; chain *C*, occupancy = 0.5).

The side chain of Tyr405, the precursor amino-acid residue which is converted to TPQ during biogenesis, adopts an orientation similar to that of TPQ in its 'on-copper' conformation in the native enzyme (Fig. 4*a*). During CAO catalysis, this conformation represents an unproductive form of TPQ, as the C5 carbonyl, which is the site of nucleophilic attack by the substrate amine, is not pointing towards the amine channel of the mature enzyme. A second conformer of the catalytic base (residue Asp319), resulting from an ∼70 ° rotation about its $C^{\beta}-C^{\gamma}$ bond, can also be observed with an occupancy of 0.5. Additional active-site residues are virtually identical in position to those observed in the native HPAO-1 structure, which was also solved to a resolution of 1.7 Å but in space group $P2_1$.

3.4. X-ray crystal structure analysis: Cu^{I}–apoHPAO-1 active site

X-ray diffraction data for apoHPAO-1 in an anaerobic complex with Cu^{I} were collected to a resolution of 1.9 Å (Table 2). Like the structure of apoHPAO-1, the active site of Cu^{I}–apoHPAO-1 contains

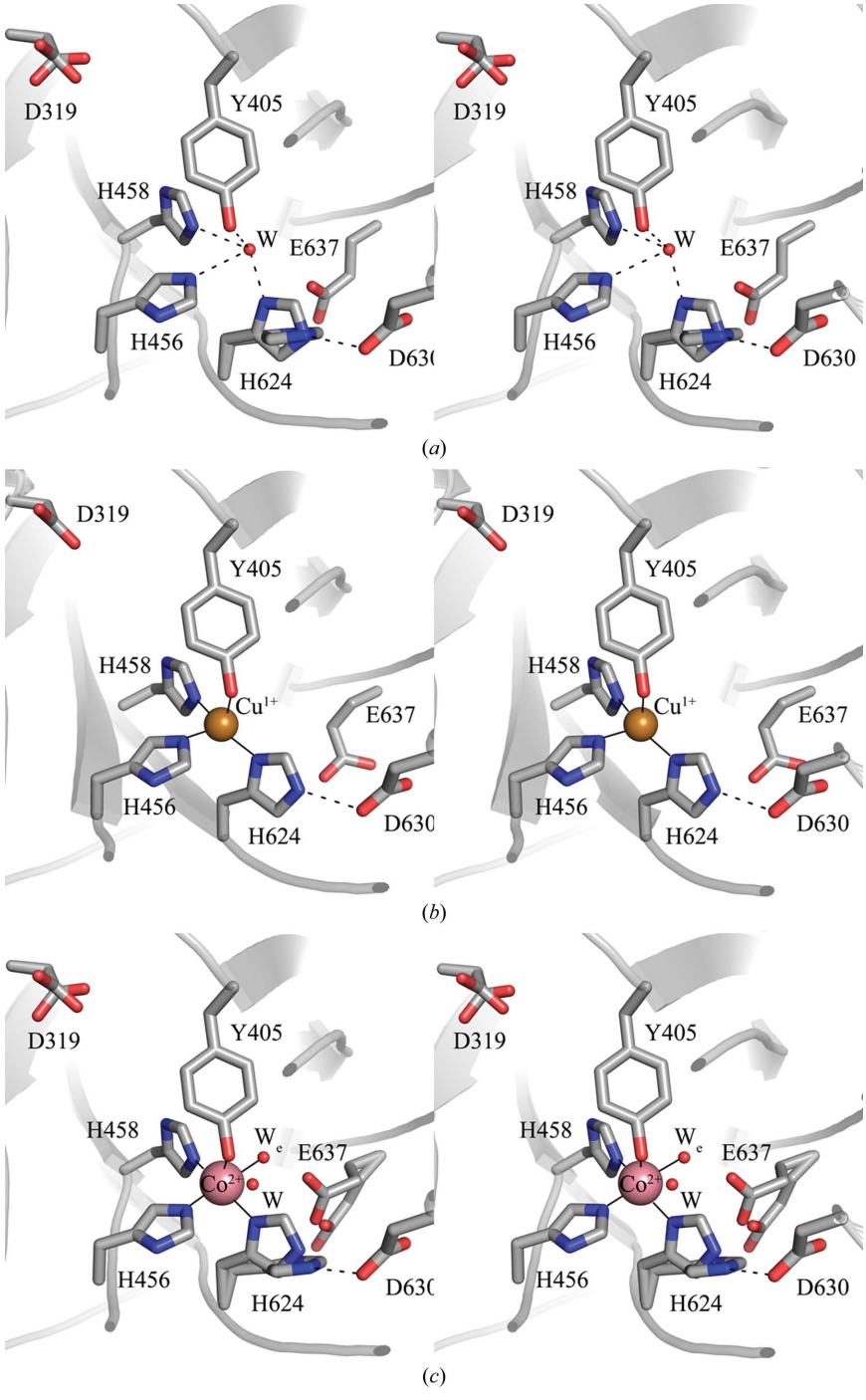

Figure 4
Stereoviews of the active-site structures of (*a*) apoHPAO-1 (chain *B*), (*b*) Cu^{I}–apoHPAO-1 (chain *A*) and (*c*) Co^{II}–apoHPAO-1 (chain *A*). Residues are shown in stick representation and are colored by atom type (carbon, gray). Metal ions are shown as spheres and are colored by atom type (Cu^{I}, gold; Co^{II}, pink). Water molecules are shown as small red spheres. Hydrogen bonds are indicated by dashed lines and ligand–metal interactions are indicated by solid lines.

the precursor amino-acid residue Tyr405 in an 'on-copper' orientation with its hydroxyl group coordinated to the Cu^{I} (Fig. 4*b*). The Cu^{I} is bound tetrahedrally and is ligated by the three conserved histidine residues, with Tyr405 serving as a fourth copper ligand at a distance of 2.8 Å. The imidazole groups of the three conserved histidine ligands all sit 2.0–2.1 Å from the bound copper ion. The tyrosine side chain is most likely to be protonated owing to the long distance between the phenolic O atom and the bound copper.

Previous structural models of HPAO-1 have not included the residues at the enzyme C-terminus owing to disorder in the electron density beyond residue 672 in the primary sequence (there are a total of 692 amino-acid residues in native HPAO-1). Electron density corresponding to residues 681–692 has been located in the Cu^{I}–apoHPAO-1 structure (Fig. 5*a*). This group of resolved residues is packed against the surface of the other monomer, adjacent to one of two β-hairpin arms which form an extensive interface between the two protein chains within one dimer (Fig. 5*b*). The Cu^{I}–apoHPAO-1 structure also contains a second interchain disulfide bond in this region that was previously unmodeled in other HPAO-1 structures (Fig. 5*c*). The disulfide bond involves residue Cys690 from one HPAO-1 monomer and residue Cys122 from its partner in the HPAO-1 dimer, forming a covalent connection between the two protein chains.

3.5. X-ray crystal structure analysis: Co^{II}–apoHPAO-1 active site

X-ray diffraction data for an aerobic complex between apo-HPAO-1 and Co^{II} were collected to a resolution of 1.27 Å, which makes this the highest resolution CAO structure to date (Table 2; for the quality of the electron density, see Fig. 6). Distances are reported as the range observed across the six polypeptides of the asymmetric unit in this crystal form following refinement. The active site of Co^{II}–apoHPAO-1 contains cobalt bound with an occupancy of 0.5 (Fig. 4*c*). The unmodified precursor tyrosine side chain ligates the cobalt, with its phenolic hydroxyl 2.15–2.20 Å away. The three histidine metal ligands sit with their imidazole groups 2.00–2.20 Å from the bound cobalt. Electron density in the $2F_o - F_c$ and $F_o - F_c$ maps indicated the presence of a water molecule acting as an equatorial ligand to the cobalt at a distance of 2.15–2.20 Å (W_e in Fig. 4*c*). Peaks in the $F_o - F_c$ electron-density map indicated the presence of a water molecule at

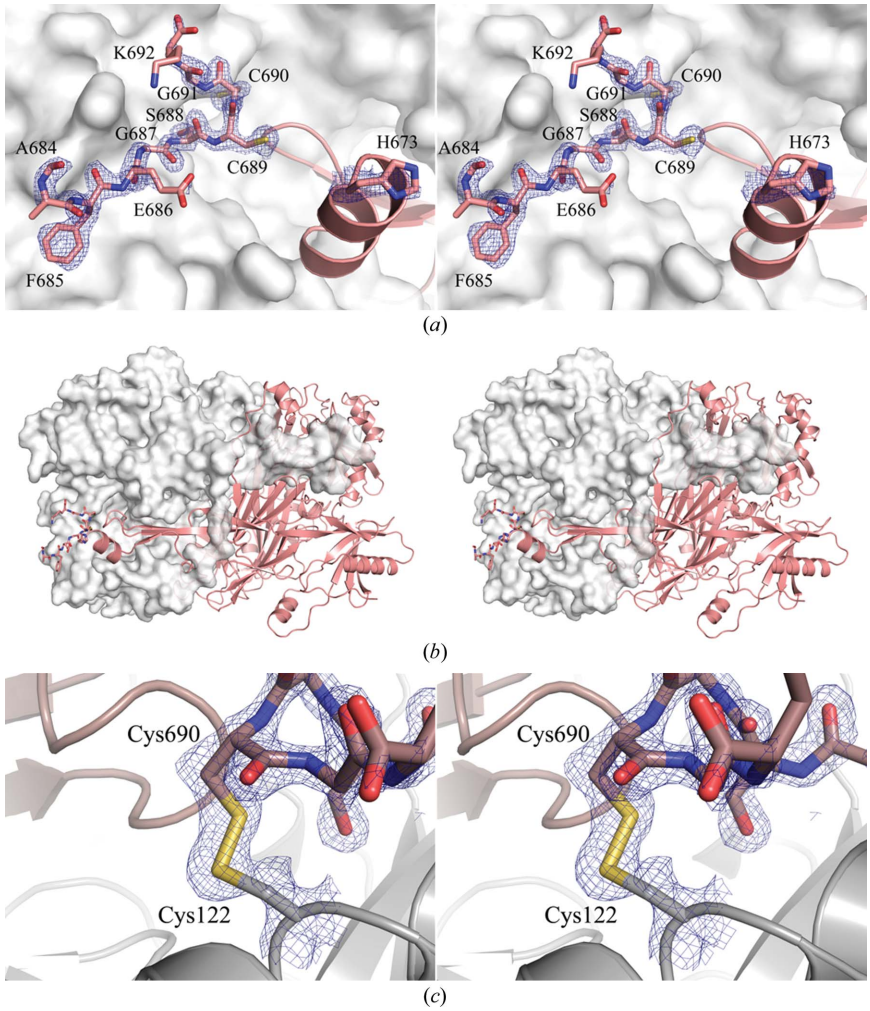

Figure 5
Stereoviews of newly modeled C-terminal residues in Cu^{I}–apoHPAO-1. (*a*) Close-up view of the new residues. One protein monomer from the HPAO-1 homodimer is shown as a gray surface and the second is shown as a pink cartoon. Newly modeled residues His673 and Ala684–Lys692 are shown in stick representation and are colored by atom type (carbon, pink). The $2F_o - F_c$ electron-density map is shown as a blue mesh and is contoured at 1σ. (*b*) Newly modeled residues in Cu^{I}–apoHPAO-1 within the context of the HPAO-1 homodimer. An HPAO-1 dimer is shown with one monomer as a gray surface and the other as a pink cartoon. New residues are shown in stick representation. (*c*) The second disulfide bond in Cu^{I}–apoHPAO-1 with $2F_o - F_c$ electron density. The HPAO-1 homodimer is shown in cartoon representation (chain *A*, gray; chain *B*, pink). Residues are shown in stick representation and are colored by atom type (gray C atoms for Cys122 in chain *A*, pink C atoms for Cys690 in chain *B*). The $2F_o - F_c$ electron-density map is shown as a blue mesh and is contoured at 1σ.

an occupancy of 0.5 between the three active-site histidine residues which is present when Co^{II} is not bound (W in Fig. 4*c*). This water molecule is nearly superimposable with that found occupying the metal-binding site in the apoHPAO-1 structure (Fig. 4*a*) and reflects the partial occupancy of the cobalt. One of the three histidine residues which ligate the active-site metal (His624) adopts the alternate conformation seen in the apoHPAO-1 structure, with its side chain rotated ∼90° around its $C^{\beta}-C^{\gamma}$ bond at different occupancies depending on the protein chain (chain *A*, occupancy = 0.3; chain *B*, occupancy = 0.5; chain *C*, occupancy = 0.4; chain *D*, occupancy = 0.3; chain *E*, occupancy = 0.4; chain *F*, occupancy = 0.4). The active-site catalytic base (Asp319) and residue Glu637 also adopt second conformations in this complex in which their side chains have rotated around the $C^{\beta}-C^{\gamma}$ bond. These alternate conformers are present at different occupancies depending on the protein chain (for Asp319, occupancy = 0.3 in all chains; for Glu637, chain *A*, occupancy = 0.5; chain *B*, occupancy = 0; chain *C*, occupancy = 0.4; chain *D*, occupancy = 0.5; chain *E*, occupancy = 0.4; chain *F*, occupancy = 0.5) and reflect the partial binding of cobalt, which results in elements of the apoHPAO-1 active site being present in the electron density.

Electron density corresponding to a group of residues near the C-terminus (residues 683–691) was observed in the $2F_o - F_c$ and $F_o - F_c$ maps of the Co^{II}–apoHPAO-1 structure. These residues are modeled at an occupancy of 0.5 and are superimposable with those modeled in the Cu^{I}–apoHPAO-1 structure (Figs. 5*a* and 5*b*).

4. Discussion

4.1. Cu^{I}–apoHPAO-1 as a physiologically relevant biogenesis intermediate

Copper in its +1 oxidation state can anaerobically bind to apoHPAO-1 and subsequent exposure of this complex to oxygen initiates TPQ formation at a rate 17-fold slower than Cu^{II}-mediated biogenesis (Samuels & Klinman, 2006). The rate-limiting step in Cu^{I}-mediated TPQ biogenesis was determined by X-band electron paramagnetic resonance spectroscopy to be the dissociation of bound superoxide from the metal site formed *via* the oxidation of Cu^{I} to Cu^{II} (Samuels & Klinman, 2006). After the oxidation of Cu^{I} to Cu^{II}, Cu^{I}-mediated biogenesis mechanistically converges with biogenesis initiated by Cu^{II}, producing indistinguishable native protein both in terms of TPQ content and catalytic rates (Samuels & Klinman, 2006).

The cellular location of HPAO-1 is the yeast peroxisome, which has implications for the electronic form of copper available to initiate TPQ biogenesis (Faber *et al.*, 1994). After translation by free cytosolic polyribosomes, proteins containing a peroxisomal targeting sequence are transported into the peroxisomal matrix after passing through a membrane-associated protein complex. The peroxisomal lumen is predicted to contain no free copper and there are no known copper transporters associated with the organelle. Given the apparent absence of copper in the peroxisome, it is thought that copper incorporation into apoHPAO-1 occurs in the cytosol while the protein is en route to its final cellular destination. Copper uptake in yeast species such as *Saccharomyces cerevisiae* involves the reduction of Cu^{II} to Cu^{I} by the cell-surface reductases Fre1 and Fre2, so it is likely that the copper available to bind to apoHPAO-1 in the yeast cytosol is in the cuprous form (Hassett & Kosman, 1995).

Samuels & Klinman note that Cu^{I} (as opposed to Cu^{II}) binding to apoHPAO-1 in the cytosol could be beneficial to the yeast, as the slower Cu^{I}-mediated biogenesis would reduce the amount of peroxide and free aldehyde generated by maturated HPAO-1 whilst in transit to the peroxisome (Samuels & Klinman, 2006). Thus, the structure of apoHPAO-1 in an anaerobic complex with Cu^{I} may represent the biologically relevant initial intermediate in terms of metal incorporation and the initiation of TPQ biogenesis for this peroxisomal CAO.

4.2. Identification of a second disulfide bond in HPAO-1

The structures of Cu^{I}–apoHPAO-1 and Co^{II}–apoHPAO-1 contain an additional disulfide bond involving Cys122 and Cys690 that was unmodeled in previous structures of HPAO-1, in which the C-terminus that contains Cys690 is disordered. HPAO-1 had previously not been modeled beyond residue Val672 in the primary sequence, with the C-terminal 20 residues missing (Li *et al.*, 1998; Chen *et al.*, 2000; Johnson *et al.*, 2007). In the Cu^{I}–apoHPAO-1 and Co^{II}–apoHPAO-1 structures the positions of residues 673–674 and 682–692 have been determined (Fig. 5). No electron density corresponding to residues 675–681 was found during refinement, suggesting that these residues remain disordered and are part of a surface-exposed loop. HPAO-1 contains 12 cysteine residues per monomer and, based on the crystal structure of native HPAO-1 (residues 18–672), contains one buried disulfide bond involving Cys338 and Cys364 (Li *et al.*, 1998). The new disulfide bond identified in the Cu^{I}–apoHPAO-1 and

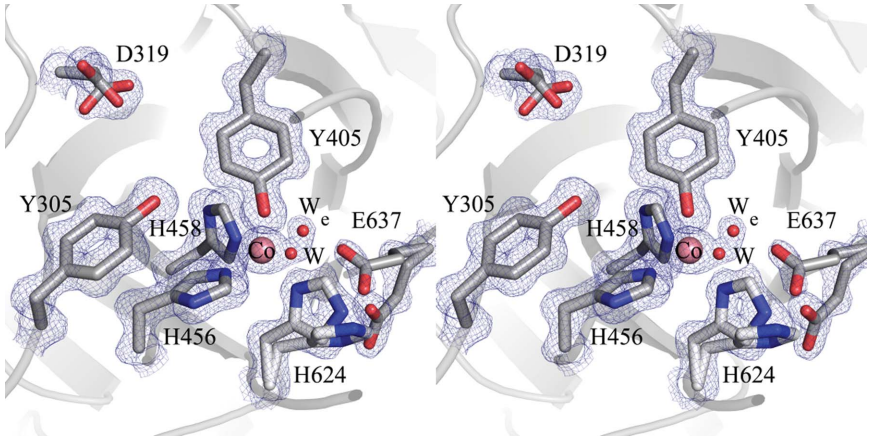

Figure 6
Stereoview of Co^{II}–apoHPAO-1 active-site residues with the $2F_o - F_c$ electron-density map. Residues are shown in stick representation and are colored by atom type (carbon, gray). The cobalt ion is shown as a pink sphere. Water molecules are shown as small red spheres. The $2F_o - F_c$ electron-density map is shown as a blue mesh and is contoured at 1σ.

Co^{II}–apoHPAO-1 structures is located at the interface between protein partners in the physiological HPAO-1 dimer and serves as a covalent link between the monomers (Fig. 5). Given that the two structures containing this new disulfide bond have been solved in different space groups, it is likely that this interaction is not a consequence of crystal contacts. There is precedent in CAO structures for disulfide bonds which covalently connect the two CAO monomers in the enzyme from *Pisum sativum*, human diamine oxidase and the human vascular adhesion protein; however, these are found in locations that are in different areas of the CAO dimer (Airenne *et al.*, 2005; Duff *et al.*, 2006; McGrath *et al.*, 2009). As the disulfide is on the surface it is likely to be reduced in the cytosol, but in HPAO-1 it could be physiological as the peroxisome is oxidizing (Aksam *et al.*, 2009).

4.3. Comparisons with other apoCAO structures

Two CAOs have been produced in their metal-free precursor (apo) forms: HPAO-1 and AGAO. The structure of apoAGAO has been solved to 2.2 Å resolution and a comparison of apoAGAO and apoHPAO-1 reveals a very similar active-site architecture (Fig. 7; Wilce *et al.*, 1997). Both active sites contain the unmodified precursor tyrosine residue arranged with its side-chain hydroxyl pointing towards the vacant metal-binding site. The active site of apoHPAO-1 contains a well ordered water molecule where the copper is normally bound which is stabilized by hydrogen-bonding interactions with the precursor tyrosine residue and two histidine imidazole ligands. In contrast, the metal-binding site of apoAGAO is empty; instead, two of the three metal-binding histidine residues (His433 and His592) have each moved ∼0.6 Å towards the vacant metal site (Fig. 7; Wilce *et al.*, 1997). In both apoCAO structures two of the three metal-binding histidine residues occupy positions identical to those in the native enzyme. The third (His624 in HPAO-1, His592 in AGAO), however, is present in two conformers, indicating that there is some flexibility in the positioning of this side chain. In apoHPAO-1 the second conformer of His624 is rotated ∼90° about its $C^{\beta}-C^{\gamma}$ bond, whereas in apoAGAO the second conformer of His592 is rotated ∼75° about its $C^{\alpha}-C^{\beta}$ bond.

In the presence of oxygen, biogenesis is initiated upon binding of copper in the apoCAO active site (Dove *et al.*, 2000). X-ray crystal structures of both apoHPAO-1 and apoAGAO in an anaerobic complex with copper have now been solved (Kim *et al.*, 2002). These two structures should contain copper in different oxidation states (although photoreduction was not tracked during the Cu^{II}–apoAGAO structure determination), with the HPAO-1 structure containing cuprous copper and the AGAO structure containing cupric copper. A comparison of the Cu^{I}–apoHPAO-1 structure with the Cu^{II}–apoAGAO complex (both solved to a resolution of 1.9 Å) reveals that despite the difference in the oxidation state of the bound copper the two structures exhibit very similar active-site architecture (Kim *et al.*, 2002). Both active sites contain the unmodified precursor tyrosine residue oriented with its hydroxyl pointing towards the bound copper. In Cu^{II}–apoAGAO, the tyrosine side chain sits with its hydroxyl ∼2.5 Å away from the Cu^{II} ion (Fig. 8; Kim *et al.*, 2002). In Cu^{I}–apoHPAO-1, the tyrosine hydroxyl is ∼2.8 Å away from the bound Cu^{I}. Both structures contain the precursor tyrosine residue in its protonated form, as inferred from the long distances between the hydroxyl of the tyrosine and bound copper. Despite the presence of copper at full occupancy, one of the three histidine residues which ligate the copper is present in two conformers in Cu^{II}–apoAGAO (His592). These are identical in position to those observed in the structure of apoAGAO (Fig. 7). In contrast, the corresponding residue in HPAO-1 only exists in the major conformer observed in structures of the native enzyme (His624). Neither of the two copper-bound active sites contains an ordered water molecule ligating the copper in an equatorial position, as has been observed in some polypeptide chains of the native HPAO-1 structure (Johnson *et al.*, 2007). It appears that a change in the oxidation state of the bound copper does not significantly alter the active-site architecture or the coordination geometry in copper-bound apoCAO. However, as noted earlier, the copper-ion oxidation state of the Cu^{II}–apoAGAO crystal structure may have changed to Cu^{I} during X-ray data collection as photoreduction was not tracked.

Like Cu^{I}, zinc is typically coordinated in buried enzyme active sites by four ligands with a tetrahedral geometry (Dudev & Lim, 2000). The structure of apoHPAO-1 in complex with Zn^{II} (PDB entry 1ekm) solved to 2.5 Å resolution contains bound zinc and active-site residues which are nearly superimposable with those of the Cu^{I}–apoHPAO-1 structure (Fig. 9; Chen *et al.*, 2000). Like Cu^{I}, Zn^{II} binds

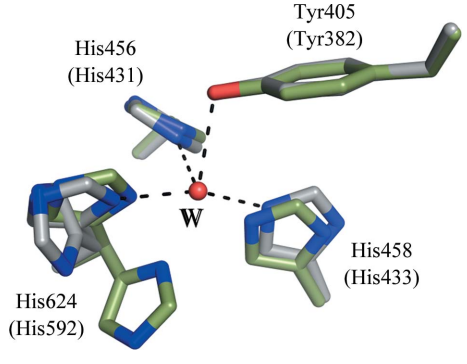

Figure 7
Overlay of the apoHPAO-1 and apoAGAO (PDB entry 1avk; Wilce *et al.*, 1997) active sites. Residues are shown in stick representation and are colored by atom type (HPAO-1, carbon, gray; AGAO, carbon, green). Residue numbering is that of HPAO-1, with equivalent residues in AGAO in parentheses. A water molecule from the apoHPAO-1 active site is shown as a red sphere and hydrogen-bonding interactions in HPAO-1 are indicated by dashed lines. Residue numbering is that of HPAO-1, with AGAO numbering in parentheses. The view is rotated ∼90° from that in Fig. 4.

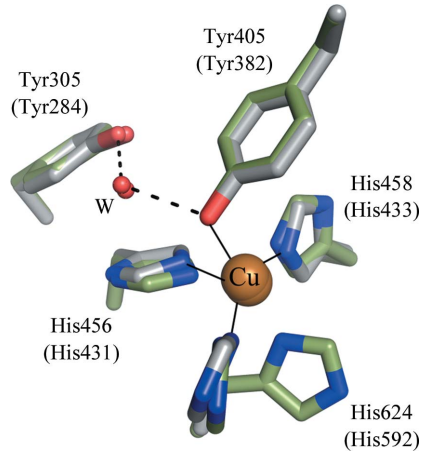

Figure 8
Overlay of the Cu^{I}–apoHPAO-1 and Cu^{II}–apoAGAO (PDB entry 1ivu; Kim *et al.*, 2002) active sites. Residues are shown in stick representation and are colored by atom type (HPAO1, carbon, gray; AGAO, carbon, green). Copper ions are shown as gold spheres and water molecules are shown as small red spheres. Hydrogen-bonding interactions in HPAO-1 are indicated by dashed lines and ligand–metal interactions in HPAO-1 are indicated by solid lines. Residue numbering is that of HPAO-1, with AGAO numbering in parentheses. Structures were aligned using *PyMOL* (http://www.pymol.org).

to the apoHPAO-1 active site in a tetrahedral geometry and is ligated by the precursor tyrosine residue as well as by the three conserved active-site histidine residues. Despite such similar coordination geometry, the binding of zinc in the active sites of CAOs renders the enzymes inert, while copper binding initiates biogenesis (Kishishita *et al.*, 2003). The specific factors which inhibit zinc-mediated biogenesis in apoCAO are unclear, but may relate to its filled *d*-orbital electron configuration.

The presence of cobalt in the AGAO active site initiates biogenesis under aerobic conditions, but cobalt does not support the production of TPQ in HPAO-1. The structures of apoHPAO-1 in complex with Co^{II} and of an anaerobic Co^{II}–apoAGAO complex have been solved to resolutions of 1.27 and 2.0 Å, respectively (Okajima *et al.*, 2005). In the case of HPAO-1 the Co^{II} complex represents an inert structure, while in AGAO the anaerobic Co^{II} complex is the first intermediate in Co^{II}-mediated biogenesis, which produces TPQ identical to that of the native enzyme (Kishishita *et al.*, 2003). Comparison of the two cobalt-containing complexes indicates that cobalt binds with distinct geometries in these two apoCAOs (Fig. 10). In the case of Co^{II}–apoHPAO-1 the cobalt ion is five-coordinate, binding in a distorted square-pyramidal geometry. The species ligating the cobalt include the precursor tyrosine residue, the three conserved active-site histidine ligands and an equatorial water molecule (W_e in Fig. 10). The structure of apoAGAO in an anaerobic complex with cobalt, however, contains four-coordinate cobalt in a distorted tetrahedral geometry ligated by the three active-site histidine residues and the precursor tyrosine residue. In addition, the crystal structure of native AGAO in complex with Co^{II} has also been solved to a resolution of 2.0 Å (PDB entry 1iqx; Kishishita *et al.*, 2003). The most pronounced change in the active site of native AGAO upon the replacement of Cu^{II} with Co^{II} is in the conformation of one of the histidine residues which ligate the Co^{II}. This residue rotates ∼60° about the $C^{\alpha}-C^{\beta}$ bond and occupies a position identical to that in the Co^{II}–apoAGAO structure. In contrast to the four-coordinate tetrahedrally bound cobalt ion in Co^{II}–apoAGAO, Co^{II}–AGAO contains six-coordinate cobalt ligated by the three histidine residues, axial and equatorial water ligands common to the native structure and an additional water molecule in an octahedral geometry. Such geometric differences may explain the inefficiency of Co^{II}–PSAO in catalyzing substrate oxidation in relation to native Cu^{II}–PSAO (Mills *et al.*, 2012). It appears that differences in metal-coordination geometry, in conjunction with additional factors such as Lewis acidity and redox potential, coordinate to determine whether a metal can initiate biogenesis as well as sustain efficient catalysis in the mature CAO. Given that cobalt can support TPQ biogenesis in AGAO but not in HPAO-1, differences in cobalt coordination are likely to influence this process.

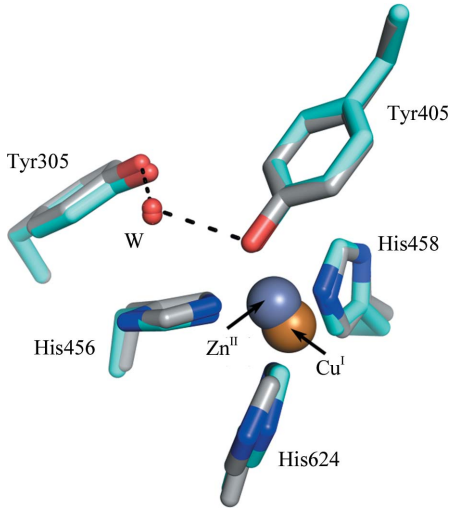

Figure 9
Overlay of the Cu^{I}–apoHPAO-1 and Zn^{II}–apoHPAO-1 (PDB code 1ekm; Chen *et al.*, 2000) active sites. Residues are shown in stick representation and are colored by atom type (Cu^{I}, carbon, gray; Zn^{II}, carbon, blue). The Cu^{I} ion is shown as a gold sphere and the Zn^{II} ion is shown as a gray sphere. Water molecules are shown as small red spheres and hydrogen-bonding interactions in Cu^{I}–apoHPAO-1 are indicated by dashed lines. Structures were aligned using *PyMOL* (http://www.pymol.org).

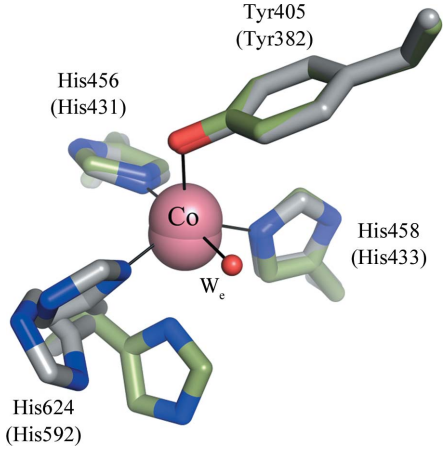

Figure 10
Overlay of the Co^{II}–apoHPAO-1 and Co^{II}–apoAGAO (PDB code 1wmp; Okajima *et al.*, 2005) active sites. Residues are shown in stick representation and are colored by atom type (HPAO-1, carbon, gray; AGAO, carbon, green). Co^{II} ions are depicted as pink spheres. A water molecule from the Co^{II}–apoHPAO-1 active site is shown as a small red sphere. Ligand–metal interactions in HPAO-1 are indicated by solid lines. Residue numbering is that of HPAO-1, with AGAO numbering in parentheses.

The authors would like to thank Dr Ke Shi and Dr Stephan Ginell for assistance with data collection and Dr Richard Welford for apoHPAO-1 protein. This work was supported by National Institutes of Health grants (GM66569 to CMW and GM039326 to JPK), Chemistry–Biology Interface Training Grant GM-008700 to BJJ, Minnesota Medical Foundation Grant 3714-9221-06, a 3M Science and Technology Graduate Fellowship to VJK, Office of the Dean of the Graduate School of the University of Minnesota Grant 21087 and a Minnesota Partnership for Biotechnology and Medical Genomics Grant SPAP-05-0013-P-FY06 to CMW. Results shown in this report are derived from work performed at Argonne National Laboratory, Structural Biology Center at the Advanced Photon Source. Argonne is operated by UChicago Argonne LLC for the US Department of Energy, Office of Biological and Environmental Research under contract DE-AC02-06CH11357.

References

Airenne, T. T., Nymalm, Y., Kidron, H., Smith, D. J., Pihlavisto, M., Salmi, M., Jalkanen, S., Johnson, M. S. & Salminen, T. A. (2005). *Protein Sci.* **14**, 1964–1974.
Aksam, E. B., de Vries, B., van der Klei, I. J. & Kiel, J. A. (2009). *FEMS Yeast Res.* **9**, 808–820.
Angelini, R., Cona, A., Federico, R., Fincato, P., Tavladoraki, P. & Tisi, A. (2010). *Plant Physiol. Biochem.* **48**, 560–564.
Cai, D. & Klinman, J. P. (1994*a*). *Biochemistry*, **33**, 7647–7653.
Cai, D. & Klinman, J. P. (1994*b*). *J. Biol. Chem.* **269**, 32039–32042.
Cai, D., Williams, N. K. & Klinman, J. P. (1997). *J. Biol. Chem.* **272**, 19277–19281.

Chen, V. B., Arendall, W. B., Headd, J. J., Keedy, D. A., Immormino, R. M., Kapral, G. J., Murray, L. W., Richardson, J. S. & Richardson, D. C. (2010). *Acta Cryst.* D**66**, 12–21.
Chen, Z., Schwartz, B., Williams, N. K., Li, R., Klinman, J. P. & Mathews, F. S. (2000). *Biochemistry*, **39**, 9709–9717.
Davidson, V. L. (2007). *Biochemistry*, **46**, 5283–5292.
Dove, J. E., Schwartz, B., Williams, N. K. & Klinman, J. P. (2000). *Biochemistry*, **39**, 3690–3698.
Drummond, J. T. & Matthews, R. G. (1994). *Biochemistry*, **33**, 3732–3741.
Dudev, T. & Lim, C. (2000). *J. Am. Chem. Soc.* **122**, 11146–11153.
Duff, A. P., Shepard, E. M., Langley, D. B., Dooley, D. M., Freeman, H. C. & Guss, J. M. (2006). *Acta Cryst.* F**62**, 1168–1173.
Dunkel, P., Gelain, A., Barlocco, D., Haider, N., Gyires, K., Sperlágh, B., Magyar, K., Maccioni, E., Fadda, A. & Mátyus, P. (2008). *Curr. Med. Chem.* **15**, 1827–1839.
Emsley, P. & Cowtan, K. (2004). *Acta Cryst.* D**60**, 2126–2132.
Faber, K. N., Haima, P., Gietl, C., Harder, W., Ab, G. & Veenhuis, M. (1994). *Proc. Natl Acad. Sci. USA*, **91**, 12985–12989.
Feng, Z., Westbrook, J. & Berman, H. M. (1998). *NUCheck*. Rutgers University, New Jersey, USA.
Gomes, L., Pereira, E. & de Castro, B. (2000). *J. Chem. Soc. Dalton Trans.*, pp. 1373–1379.
Green, J., Haywood, G. W. & Large, P. J. (1983). *Biochem. J.* **211**, 481–493.
Hassett, R. & Kosman, D. J. (1995). *J. Biol. Chem.* **270**, 128–134.
Janes, S. M., Mu, D., Wemmer, D., Smith, A. J., Kaur, S., Maltby, D., Burlingame, A. L. & Klinman, J. P. (1990). *Science*, **248**, 981–987.
Jiang, Z. J., Richardson, J. S. & Yu, P. H. (2008). *Neuropathol. Appl. Neurobiol.* **34**, 194–204.
Johnson, B. J., Cohen, J., Welford, R. W., Pearson, A. R., Schulten, K., Klinman, J. P. & Wilmot, C. M. (2007). *J. Biol. Chem.* **282**, 17767–17776.
Kim, M., Okajima, T., Kishishita, S., Yoshimura, M., Kawamori, A., Tanizawa, K. & Yamaguchi, H. (2002). *Nature Struct. Mol. Biol.* **9**, 591–596.
Kishishita, S., Okajima, T., Kim, M., Yamaguchi, H., Hirota, S., Suzuki, S., Kuroda, S., Tanizawa, K. & Mure, M. (2003). *J. Am. Chem. Soc.* **125**, 1041–1055.
Laskowski, R. A., MacArthur, M. W., Moss, D. S. & Thornton, J. M. (1993). *J. Appl. Cryst.* **26**, 283–291.
Li, R., Chen, L., Cai, D., Klinman, J. P. & Mathews, F. S. (1997). *Acta Cryst.* D**53**, 364–370.
Li, R., Klinman, J. P. & Mathews, F. S. (1998). *Structure*, **6**, 293–307.
Matsuzaki, R., Fukui, T., Sato, H., Ozaki, Y. & Tanizawa, K. (1994). *FEBS Lett.* **351**, 360–364.
McGrath, A. P., Caradoc-Davies, T., Collyer, C. A. & Guss, J. M. (2010). *Biochemistry*, **49**, 8316–8324.
McGrath, A. P., Hilmer, K. M., Collyer, C. A., Shepard, E. M., Elmore, B. O., Brown, D. E., Dooley, D. M. & Guss, J. M. (2009). *Biochemistry*, **48**, 9810–9822.
McNicholas, S., Potterton, E., Wilson, K. S. & Noble, M. E. M. (2011). *Acta Cryst.* D**67**, 386–394.
Mills, S. A., Brown, D. E., Dang, K., Sommer, D., Bitsimis, A., Nguyen, J. & Dooley, D. M. (2012). *J. Biol. Inorg. Chem.* **17**, 507–515.
Murshudov, G. N., Skubák, P., Lebedev, A. A., Pannu, N. S., Steiner, R. A., Nicholls, R. A., Winn, M. D., Long, F. & Vagin, A. A. (2011). *Acta Cryst.* D**67**, 355–367.
Obata, T. (2006). *Life Sci.* **79**, 417–422.
Okajima, T., Kishishita, S., Chiu, Y.-C., Murakawa, T., Kim, M., Yamaguchi, H., Hirota, S., Kuroda, S. & Tanizawa, K. (2005). *Biochemistry*, **44**, 12041–12048.
Otwinowski, Z. & Minor, W. (1997). *Methods Enzymol.* **276**, 307–326.
Puig, S. & Thiele, D. J. (2002). *Curr. Opin. Chem. Biol.* **6**, 171–180.
Salmi, M., Yegutkin, G. G., Lehvonen, R., Koskinen, K., Salminen, T. & Jalkanen, S. (2001). *Immunity*, **14**, 265–276.
Samuels, N. M. & Klinman, J. P. (2005). *Biochemistry*, **44**, 14308–14317.
Samuels, N. M. & Klinman, J. P. (2006). *J. Biol. Chem.* **281**, 21114–21118.
Schwartz, B., Dove, J. E. & Klinman, J. P. (2000). *Biochemistry*, **39**, 3699–3707.
Shen, S. H., Wertz, D. L. & Klinman, J. P. (2012). *PLoS One*, **7**, e29270.
Vaguine, A. A., Richelle, J. & Wodak, S. J. (1999). *Acta Cryst.* D**55**, 191–205.
Wilce, M. C., Dooley, D. M., Freeman, H. C., Guss, J. M., Matsunami, H., McIntire, W. S., Ruggiero, C. E., Tanizawa, K. & Yamaguchi, H. (1997). *Biochemistry*, **36**, 16116–16133.
Winn, M. D. *et al.* (2011). *Acta Cryst.* D**67**, 235–242.